Multibeam Seeded Brillouin Sidescatter in Inertial Confinement Fusion Experiments

D. Turnbull,* P. Michel, J. E. Ralph, L. Divol, J. S. Ross, L. F. Berzak Hopkins, A. L. Kritcher, D. E. Hinkel, and J. D. Moody
Lawrence Livermore National Laboratory, Livermore, California 94550, USA
(Received 7 January 2015; published 26 March 2015)

We present the first observations of multibeam weakly seeded Brillouin sidescatter in indirect-drive inertial confinement fusion (ICF) experiments. Two seeding mechanisms have been identified and quantified: specular reflections ("glint") from opposite hemisphere beams, and Brillouin backscatter from neighboring beams with a different angle of incidence. Seeded sidescatter can dominate the overall coupling losses, so understanding this process is crucial for proper accounting of energy deposition and drive symmetry. Glint-seeded scattered light could also be used to probe hydrodynamic conditions inside ICF targets.

DOI: 10.1103/PhysRevLett.114.125001 PACS numbers: 52.57.-z, 52.38.Bv

Inertial confinement fusion (ICF) experiments seek to achieve controlled thermonuclear burn in the laboratory by using a large number of high energy lasers to heat and compress a target containing nuclear fuel. In indirect-drive ICF, the lasers are fired onto the inner surface of a high-Z cylindrical cavity (hohlraum) through laser entrance holes on either end. The cavity creates a uniform radiation bath that drives a spherical capsule containing the fuel in the center of the target [1,2]. Direct-drive ICF eliminates the hohlraum, instead using the lasers to irradiate the capsule directly [3,4]. In both cases, the presence of many overlapping beams leads to complex multibeam laser-plasma interactions [5]. These include crossed-beam energy transfer (CBET) [6–13], which can redistribute laser energy, alter drive symmetry, and modify hydrodynamic conditions, the common-wave two plasmon decay instability [14,15], which produces hot electrons that can cause deleterious fuel preheat, and backscatter reamplification [16], which can increase overall laser coupling losses. Understanding, and in some cases mitigating, these endemic processes is essential for optimizing ICF implosions.

In this Letter, we report the first observations of multibeam weakly seeded Brillouin sidescatter in indirect-drive experiments. The process is illustrated in Fig. 1: a small-amplitude electromagnetic "seed" is amplified by multiple "pump" laser beams via stimulated Brillouin scattering (SBS) in a nearly counterpropagating geometry. As a result, the scattered light observed in the direction of a particular beam (that coincides with the direction of the seed) can be comprised mostly of side-scattered light from other beams. Two different seeding mechanisms have been identified and quantified: (i) Brillouin backscatter from neighboring beams with a different angle of incidence, and (ii) specular reflections ("glint") from opposite hemisphere beams. Sidescatter can dominate the overall coupling losses from indirect-drive ICF targets.

All experiments were conducted at the National Ignition Facility (NIF). At NIF, 192 laser beams are grouped first into quadruplets ("quads") of four beams, and, subsequently, into four cones that each have a different angle of incidence on the hohlraum wall. The two "inner" cones, with 23.5° and 30° incidence, illuminate the center of the target and drive the capsule from the hohlraum waist. The "outer" cones, with 44.5° and 50° incidence, drive the capsule from the poles. The inners and outers are carefully

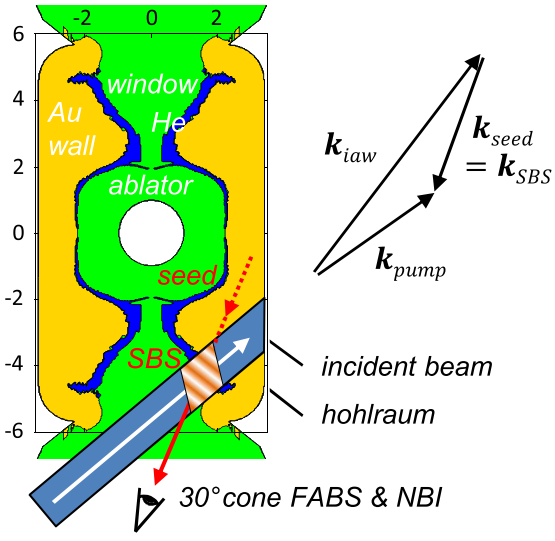

FIG. 1 (color online). This illustrates seeded SBS in a hohlraum. A seed may be amplified by one or more quads in a near-backscatter geometry prior to exiting the hohlraum. The direction of the scattered light is fixed by the direction of the seed. It is subsequently observed using the 30° cone scattered light diagnostics. The seed source, direction, and overlap region with incident outer beams are shown approximately, overlaid with the material boundary surfaces predicted by hydrodynamic simulations for a shot and time—N140429-004-999 at 5.5 ns—analyzed throughout the Letter.

balanced for symmetric implosions, which minimizes residual kinetic energy and maximizes fusion yield [17–19]. The experiments reported here were realized in "near-vacuum hohlraums (NVH)," which contain an initial gas fill of 0.032 mg/cc He. They were driven with relatively short laser pulses of 6–7 ns duration delivering two carefully timed shocks. Although a typical NVH drive raises the fuel entropy (reducing compressibility) more than optimized designs with 3–4 shock laser pulses in gas-filled hohlraums (with 0.96–1.6 mg/cc He) [20,21], the more efficient x-ray drive [22–24] and lower coupling losses of the NVH [25] allow for ignition relevant designs.

The scattered light is diagnosed using the NIF full aperture backscatter (FABS) and near backscatter imager (NBI) diagnostics [26]. FABS samples light that is recollected by the focusing optics of a 30° and a 50° quad in the lower hemisphere, which is typically assumed to be direct backscatter from each quad's incident light. The light is temporally and spectrally resolved using fast diodes and streaked spectrometers. NBI is used to assess the scattered light that isn't collected by the final optics (generally backscatter with a somewhat larger divergence than the incident light). It consists of large scatter plates inside the target chamber that are imaged through an opposing port.

Figure 2(a) shows a typical time-resolved spectrum of SBS observed with the 30° FABS on a NVH target. This light usually amounts to 1%–4% of total laser energy and often dominates the total coupling losses. The scattered light has two distinct spectral features associated with two different sidescatter seeding mechanisms. The first is redshifted with respect to the incident laser wavelength, corresponding to a SBS seed. The other is blueshifted and is seeded by glint. Sidescatter can be more significant than direct backscatter in these targets because the seed amplitudes may be $\approx 10^5$–10^7 times larger than the thermal noise levels from which scattered light is usually assumed to grow [27]. Each seeding mechanism is described in more detail in the remainder of this Letter.

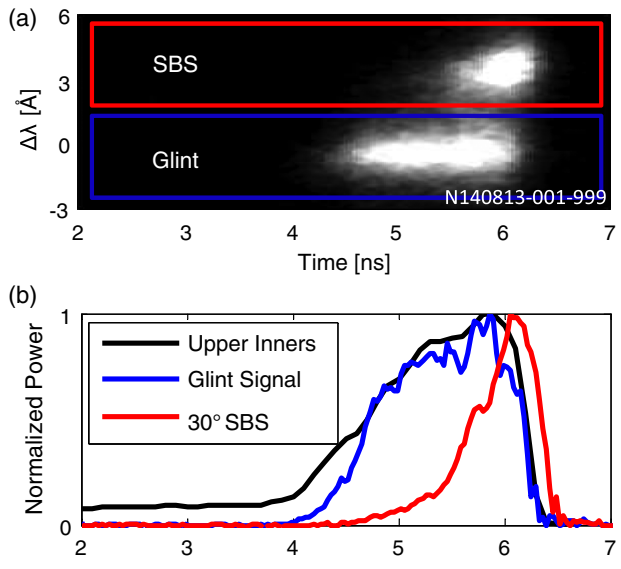

FIG. 2 (color online). (a) A typical SBS spectrum observed with the 30° FABS. There are two distinct features: (i) that which is redshifted with respect to the incident light has been determined to be mostly sidescatter seeded by SBS backscatter, and (ii) that which is blueshifted is sidescatter seeded by glint. (b) Normalized lineouts through each feature plotted with the upper hemisphere normalized incident power. The glint-seeded feature turns off with the upper hemisphere beams whereas the SBS-seeded feature continues until the end of the lower hemisphere.

Seeding by SBS from neighboring beams.— The redshifted scattered light observed in Fig. 2(a) has all of the "usual" features of direct backscatter from the diagnosed 30° incidence quad; for example, the scattered light is spatially localized within the incident laser beams' apertures. However, we have established that this light is in fact merely seeded by direct backscatter from the diagnosed quad and subsequently reamplified by neighboring beams, which actually supply most of the energy. To prove this, an experiment was conducted in which the outer beams from the lower hemisphere were truncated 800 ps prior to all other NIF beams. The result is shown in Fig. 3. The redshifted feature, isolated using the streaked spectral data, was reduced to $7\% \pm 2\%$ of the peak value just prior to truncation, indicating that most ($\approx$93%) of the energy in the signal was actually provided by outer beams. Note that the drop occurs on a time scale (< 100 ps) that is too short to be caused by a sudden change in hydrodynamic conditions due to the absence of the outer beams. This process is similar to multibeam backscatter amplification, which was proposed in Ref. [16] for stimulated Raman scattering. This work constitutes the first experimental demonstration of this process for SBS.

Seeding by glint from the opposite hemisphere.— The second seeding mechanism is glint from opposite

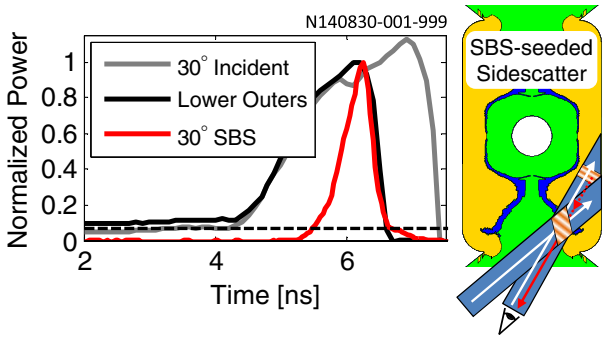

FIG. 3 (color online). A lineout through the SBS is overplotted with the truncated lower outer beam power and the full length 30° pulse. The SBS drops to about $7\% \pm 2\%$ of the peak value just prior to truncation, indicating the outers were reamplifying the inner SBS by about 14×. The accompanying illustration shows the inner SBS seed (red dashed) from lower inner beams getting reamplified by lower outer beams before exiting the hohlraum.

hemisphere beams. In indirect-drive ICF, glint generally refers to early time specular reflections from the hohlraum wall [28], although in this case glint is observed toward the end of the laser drive. Inner cone glint can exit the hohlraum through the opposing laser entrance hole. The hohlraum wall acts like a cylindrical focusing optic, which allows the extreme glint rays from an upper hemisphere 23.5° quad to reach the lower hemisphere 30° cone scattered light diagnostics. This is shown in Fig. 4. We identify scattered light seeded by glint using several observables. First, the spectrum is blueshifted relative to the incident laser [e.g., Fig. 2(a)], which is due to the Doppler shift imparted by the expanding wall as well as the fact that the hohlraum plasma density is increasing with time [29,30]. Second, it has a diffuse distribution atypical of Brillouin backscatter but fairly well matched by ray tracing of the upper hemisphere quad expected to reach FABS/NBI as shown in Figs. 4(c) and 4(d) for a particular shot at 5.5 ns. Third, FABS polarimetry indicates the glint has a mixed polarization due to spatial smearing and collection of light from multiple beams, whereas SBS generally retains the incident beam polarization to first order [31]. The ultimate check was made by truncating the beams from the upper hemisphere 200 ps early, as shown in Fig. 2(b). The blueshifted feature disappeared as the inner beams from the upper hemisphere turned off, confirming that glint was the source of the signal. Note that the redshifted feature was unaffected and continued until the end of the remaining beams.

To test whether late time glint signals are pure specular reflections or merely a seed for Brillouin sidescatter, the outer beams in the lower hemisphere were truncated 800 ps early in another experiment. Figure 5 shows that the glint was reduced to $45 \pm 5\%$ of the peak value, indicating in this case that the lower hemisphere outer beams were providing about half of the energy in the signal at that time. This confirmed that glint is a second seeding mechanism for SBS sidescatter. Note that this amplification is a minimum value, because the upper hemisphere glint may also seed sidescatter from the lower hemisphere inner beams.

Amplified glint is qualitatively very similar to "crossed-beam energy transfer" (CBET) in direct-drive experiments (see Ref. [5] and references therein), in that residual unabsorbed light seeds Brillouin sidescatter of other incident beams. Increased backscatter reflectivity due to electromagnetic seeding has also been observed in other target geometries [32,33]. This work is distinguished by the indirect-drive hohlraum geometry and the observed predominance of sidescatter over backscatter.

Figure 6 shows the time history of the blueshifted (glint) component of the scattered light on the shot also shown in Fig. 4. It is plotted as a reflectivity, i.e., the fraction of the incident inner beams escaping the hohlraum. The early time inner cone glint reflectivity, initially ≈15%, decays rapidly with time. Close to the onset of the laser, the signal is likely a pure specular reflection, and its decrease is expected because the gold is expanding away from the wall, increasing the plasma density scale length near the turning point and therefore the inverse bremsstrahlung absorption of the incident beams. However, the glint signals rebound at late time during peak power, at which point the apparent

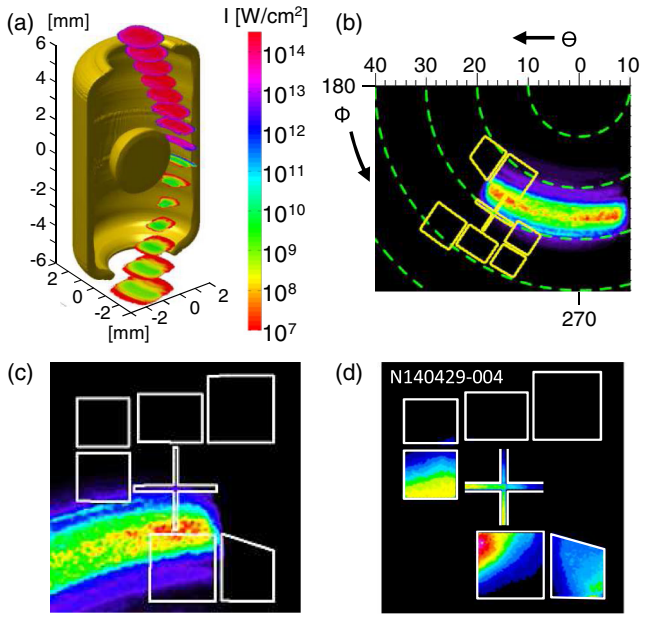

FIG. 4 (color online). (a) The calculated intensity of a 23.5° quad after reflection ($R \approx 3 \times 10^{-6}$) off of the $0.16 n_c$ density contour provided by HYDRA for shot N140429-004-999 at 5.5 ns. (b) The calculated distribution in theta-phi space when the light reaches the chamber wall, plotted with yellow quadrangles that indicate the positions of the 30° NBI scatter plates. (c) The same thing from the face-on view of NBI, and (d) shows the actual distribution of light on the NBI plates on that shot. The data are slightly broader in theta and narrower in phi than the simulation.

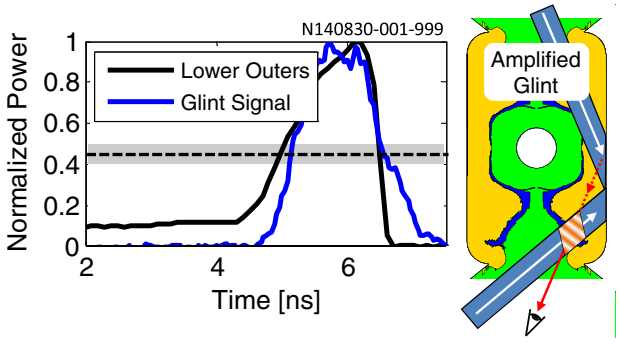

FIG. 5 (color online). A lineout through the glint is overplotted with the truncated lower outer beam power. The glint drops by a factor of ≈2, indicating the outers were providing about half the energy. The accompanying illustration shows glint from upper inner beams intercepting the lower outers entering the hohlraum in a region (with outward sonic flow) that supports energy transfer from the incoming to the outgoing light.

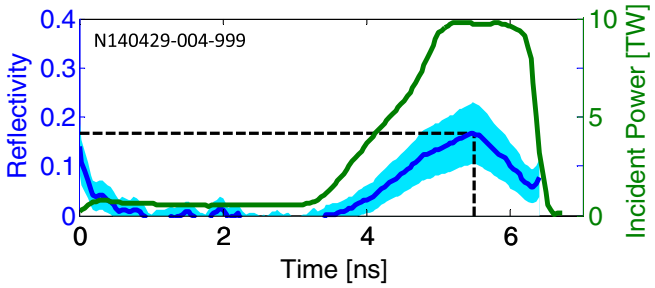

FIG. 6 (color online). The apparent "reflectivity" inferred from the data is plotted with the incident laser pulse shape, which uses the time history from FABS, total energy from the NBI plate, and ray tracing to determine a multiplier with which to extrapolate a total signal. The early time reflectivity decays rapidly but at peak power glint returns and at 5.5 ns (the time corresponding to the hydrodynamic simulation in Fig. 4), the reflectivity exceeds the value at time zero.

reflectivity can approach or even exceed the early time value. For the shot shown in Figs. 4 and 6, late time glint amounted to a coupling loss of $2.3\% \pm 0.5\%$ of the total laser energy. The large amplitude at late time is partially explained by the previous finding that glint can seed SBS sidescatter. However, since the amplification was modest ($\approx 2\times$), the actual late time glint reflectivity is likely at least 10^{-3}–10^{-2}.

The diagnostic potential of glint.— Glint can carry signatures of its propagation through the hohlraum, and several features (including its amplitude) appear to highlight inaccurate features of the hydrodynamic simulations. Figure 4(a) shows a density contour surface close to $0.16n_c$ at 5.5 ns (coinciding with the signal peak) for the shot in question. This surface is the expected turning point for a 23.5° incidence quad (n_c is the critical density for 351 nm light) [34]. Ray tracing performed on this map confirms there is still a pathway through the hohlraum for glint, but the calculations predict a reflectivity of $\approx 3 \times 10^{-6}$ that is much below the inferred value. The implication of this discrepancy is that the turning point of the inner beams near the waist likely has a steeper density gradient and higher temperature than predicted by hydrodynamic simulations. The steeper density gradient is bolstered by an additional discrepancy between the predicted and observed azimuthal extent of the scattered light [cf. Figs. 4(c) and 4(d)]. In order to qualitatively reproduce the data, ray tracing calculations suggest the $0.16n_c$ contour is at a radius that is 300 μm larger than the simulation, which implies it has only moved 1/3 as far as expected. The ongoing challenge of accurately modeling late time inner beam propagation in NVH in order to reproduce implosion symmetry further reinforces the likelihood that glint is exposing real errors in the hydrodynamic simulations [35].

Glint has also been used to confirm the absence of CBET in NVH experiments (when all of the beams have the same wavelength, unlike gas-filled experiments where a wavelength shift is used to control CBET for symmetry tuning). This was verified by truncating the outer beams in the upper hemisphere early and observing no effect on the glint signal measured in the lower hemisphere. This also eliminates CBET as a possible alternative explanation for the scattered light signal reductions shown previously (cf. Figs. 3 and 5).

In summary, we present evidence of multibeam weakly seeded Brillouin sidescatter in indirect-drive ICF experiments. With near-vacuum hohlraum platforms, a majority of the scattered light appearing on inner cone backscatter diagnostics is actually outer beam sidescatter seeded by glint and Brillouin backscatter from inner beams. The scattered light diagnostics, which were designed to measure backscatter and near backscatter, capture a relatively narrow slice of the diffuse glint-seeded scattered light. These experiments have helped clarify the sources and total amplitude of the observed signals and have thereby improved our modeling of the implosions. Glint has also demonstrated its diagnostic potential by exposing inaccurate features of the hydrodynamic simulations and by facilitating a measurement of crossed-beam energy transfer.

D. T. would like to thank Nino Landen, Nathan Meezan, and Marilyn Schneider for comments and feedback, as well as Jay Salmonson and Steve MacLaren for allowing ride-along experiments to be conducted within their campaign. This work was performed under the auspices of the U.S. Department of Energy by Lawrence Livermore National Laboratory under Contract No. DE-AC52-07NA27344.

*turnbull2@llnl.gov

[1] J. Lindl, Phys. Plasmas **2**, 3933 (1995).
[2] J. Lindl, P. Amendt, R. Berger, S. Glendinning, S. Glenzer, S. Haan, R. Kauffman, O. Landen, and L. Suter, Phys. Plasmas **11**, 339 (2004).
[3] S. Bodner, D. Colombant, J. Gardner, R. Lehmberg, S. Obenschain, L. Phillips, A. Schmitt, J. Sethian, R. McCrory, W. Seka, C. Verdon, J. Knauer, B. Afeyan, and H. Powell, Phys. Plasmas **5**, 1901 (1998).
[4] P. McKenty, V. Goncharov, R. Town, S. Skupsky, R. Betti, and R. McCrory, Phys. Plasmas **8**, 2315 (2001).
[5] J. F. Myatt, J. Zhang, R. W. Short, A. V. Maximov, W. Seka, D. H. Froula, D. H. Edgell, D. T. Michel, I. V. Igumenshchev, D. E. Hinkel, P. Michel, and J. D. Moody, Phys. Plasmas **21**, 055501 (2014).
[6] W. L. Kruer, S. C. Wilks, B. B. Afeyan, and R. K. Kirkwood, Phys. Plasmas **3**, 382 (1996).
[7] J. D. Moody *et al.*, Nat. Phys. **8**, 344 (2012).
[8] P. Michel, L. Divol, E. A. Williams, S. Weber, C. A. Thomas, D. A. Callahan, S. W. Haan, J. D. Salmonson, S. Dixit, D. E. Hinkel, M. J. Edwards, B. J. MacGowan, J. D. Lindl, S. H. Glenzer, and L. J. Suter, Phys. Rev. Lett. **102**, 025004 (2009).
[9] P. Michel, L. Divol, E. A. Williams, C. A. Thomas, D. A. Callahan, S. Weber, S. W. Haan, J. D. Salmonson, N. B. Meezan, O. L. Landen, S. Dixit, D. E. Hinkel,

M. J. Edwards, B. J. MacGowan, J. D. Lindl, S. H. Glenzer, and L. J. Suter, Phys. Plasmas **16**, 042702 (2009).
[10] C. J. Randall, J. R. Albritton, and J. J. Thomson, Phys. Fluids **24**, 1474 (1981).
[11] I. V. Igumenshchev, D. H. Edgell, V. N. Goncharov, J. A. Delettrez, A. V. Maximov, J. F. Myatt, W. Seka, A. Shvydky, S. Skupsky, and C. Stoeckl, Phys. Plasmas **17**, 122708 (2010).
[12] I. V. Igumenshchev *et al.*, Phys. Plasmas **19**, 056314 (2012).
[13] P. Michel, W. Rozmus, E. A. Williams, L. Divol, R. L. Berger, R. P. J. Town, S. H. Glenzer, and D. A. Callahan, Phys. Rev. Lett. **109**, 195004 (2012).
[14] C. Stoeckl, R. E. Bahr, B. Yaakobi, W. Seka, S. P. Regan, R. Craxton, J. Delettrez, R. Short, J. Myatt, A. V. Maximov, and H. Baldis, Phys. Rev. Lett. **90**, 235002 (2003).
[15] D. T. Michel, A. V. Maximov, R. W. Short, S. X. Hu, J. F. Myatt, W. Seka, A. A. Solodov, B. Yaakobi, and D. H. Froula, Phys. Rev. Lett. **109**, 155007 (2012).
[16] R. K. Kirkwood *et al.*, Phys. Plasmas **18**, 056311 (2011).
[17] A. Kritcher, R. Town, D. Bradley, D. Clark, B. Spears, O. Jones, S. Haan, P. Springer, J. Lindl, R. Scott, D. Callahan, M. Edwards, and O. Landen, Phys. Plasmas **21**, 042708 (2014).
[18] B. Spears, M. Edwards, S. Hatchett, J. Kilkenny, J. Knauer, A. Kritcher, J. Lindl, D. Munro, P. Patel, H. Robey, and R. Town, Phys. Plasmas **21**, 042702 (2014).
[19] R. Town *et al.*, Phys. Plasmas **21**, 056313 (2014).
[20] T. R. Dittrich, O. A. Hurricane, D. A. Callahan, E. L. Dewald, T. Doppner, D. E. Hinkel, L. F. Berzak Hopkins, S. Le Pape, T. Ma, J. L. Milovich, J. C. Moreno, P. K. Patel, H.-S. Park, B. A. Remington, J. D. Salmonson, and J. L. Kline, Phys. Rev. Lett. **112**, 055002 (2014).
[21] S. Haan *et al.*, Phys. Plasmas **18**, 051001 (2011).
[22] A. J. MacKinnon *et al.*, Phys. Plasmas **21**, 056318 (2014).
[23] R. Kauffman, L. Powers, S. Dixit, S. Glendinning, S. Glenzer, R. Kirkwood, O. Landon, B. MacGowan, J. Moody, T. Orzechowski, D. Pennington, G. Stone, L. Suter, R. Turner, T. Weiland, A. Richard, and M. Blain, Phys. Plasmas **5**, 1927 (1998).
[24] L. Suter, R. Kauffman, C. Darrow, A. Hauer, H. Kornblum, O. Landen, T. Orzechowski, D. Phillion, J. Porter, L. Powers, A. Richard, M. Rosen, A. Thiessen, and R. Wallace, Phys. Plasmas **3**, 2057 (1996).
[25] S. Le Pape, L. Divol, L. Berzak Hopkins, A. Mackinnon, N. B. Meezan, D. Casey, J. Frenje, H. Herrmann, J. McNaney, T. Ma, K. Widmann, A. Pak, G. Grimm, J. Knauer, R. Petrasso, A. Zylstra, H. Rinderknecht, M. Rosenberg, M. Gatu-Johnson, and J. D. Kilkenny, Phys. Rev. Lett. **112**, 225002 (2014).
[26] J. D. Moody *et al.*, Rev. Sci. Instrum. **81**, 10D921 (2010).
[27] R. K. Kirkwood, B. J. MacGowan, D. S. Montgomery, B. B. Afeyan, W. L. Kruer, D. M. Pennington, S. C. Wilks, J. D. Moody, K. Wharton, C. A. Back, K. G. Estabrook, S. H. Glenzer, M. A. Blain, R. L. Berger, D. E. Hinkel, B. F. Lasinski, E. A. Williams, D. Munro, B. H. Wilde, and C. Rousseaux, Phys. Plasmas **4**, 1800 (1997).
[28] H. Honda, H. Nishimura, S. Miyamoto, D. Ohnuki, K. Fujita, Y. Ochi, H. Miki, H. Takabe, S. Nakai, and K. Mima, Plasma Phys. Controlled Fusion **40**, 1097 (1998).
[29] T. Dewandre, J. Albritton, and E. Williams, Phys. Fluids **24**, 528 (1981).
[30] K. Tanaka, L. Goldman, W. Seka, R. Short, and E. Williams, Phys. Fluids **27**, 2960 (1984).
[31] D. Turnbull, J. Moody, P. Michel, J. Ralph, and L. Divol, Rev. Sci. Instrum. **85**, 11E603 (2014).
[32] J. C. Fernández, B. S. Bauer, K. S. Bradley, J. A. Cobble, D. S. Montgomery, R. G. Watt, B. Bezzerides, K. G. Estabrook, R. Focia, S. R. Goldman, D. B. Harris, E. L. Lindman, H. A. Rose, J. Wallace, and B. H. Wilde, Phys. Rev. Lett. **81**, 2252 (1998).
[33] W. Seka, H. A. Baldis, J. Fuchs, S. P. Regan, D. D. Meyerhofer, C. Stoeckl, B. Yaakobi, R. S. Craxton, and R. W. Short, Phys. Rev. Lett. **89**, 175002 (2002).
[34] W. L. Kruer *et al.*, *The Physics of Laser Plasma Interactions* (Addison-Wesley, New York, 1988), Vol. 70.
[35] L. Hopkins, Bull. Am. Phys. Soc. **59**, 236 (2014).